Night-sky spectral atlas of OH emission lines in the near-infrared

P. Rousselot[1]**, C. Lidman**[2]**, J.-G. Cuby**[2]**, G. Moreels**[1]**, and G. Monnet**[3]

[1] Observatory of Besançon, B.P. 1615, 25010 Besançon Cedex, France
[2] ESO, Alonso de Cordova 3107, Vitacura, Casilla 19001, Santiago 19, Chile
[3] ESO, Karl-Schwarzschild-Strasse 2, 85748 Garching bei München, Germany

Abstract. In this paper, we present medium resolution spectra of the night-sky OH emission. The spectra cover the range 0.997 – 2.25 μm with a resolution of about 8000. Line wavelengths are computed from laboratory data and are given in vacuum. A few lines due to O_2 are also identified.

This new set of data can be used to calibrate the wavelength scale of spectra obtained in the near-infrared. It can also help to distinguish between the lines due to astronomical objects and lines due to the earth atmosphere.

Key words: line: identification

1. Introduction

Emission lines produced by the OH radical dominate near-infrared spectra. They appear between 0.61 and 2.62 μm, and correspond to transitions with $\Delta v = 2$ to 5. The brightest lines appear above 1.5 μm (see Fig. 1). The absolute intensities of these lines are strongly time dependent. This is caused by waves in the upper atmosphere. The relative intensities are also time dependent.

The OH radicals are created in an atmospheric layer of 6–10 km thickness at an altitude of about 87 km. They are created in a reaction between atomic hydrogen and ozone. The energy budget of the reaction allows the OH radical to be populated up to the $X^2\Pi_i$ $v = 9$ level (Anlauf et al. 1968).

The removal of these lines from astronomical spectra is an essential part of the processing of near-infrared spectral data. As the flux within these lines is several orders of magnitude above the sky emission from other sources, they are the dominant source of noise in fully processed data. Nevertheless, since the OH lines provide in-situ references for wavelength calibration in the near-infrared domain, a detailed atlas of OH lines with accurate wavelengths and reasonable relative intensities allows direct wavelength calibration on the sky spectra

The most recent work dedicated to the study of the night-sky emission lines was limited to the range 3850–10600 Å (Osterbrock et al. 1996, 1997 and 1998). This work was based on data obtained by the Keck 10-m telescope on Mauna Kea and the

---

Send offprint requests to: P. Rousselot

high-resolution spectrograph (HIRES). Spectra of the night airglow emission in the 1.2 and 2.5 μm (Gush & Buijs 1964) and 3–4 μm (Bunn & Gush 1972) ranges were obtained by using balloon-borne Fourier transform spectrometers. More recently Maihara et al. (1993) and Oliva & Origlia (1992) published also some experimental data concerning the atmospheric OH lines. Some interesting data are also available thanks to the web server of several optical or infrared observatories. The aim of the present paper is to extend the atlas of Osterbrock et al. (1996, 1997), to the 1 – 2.25 μm domain.

2. Observational data

The data presented in this paper have been obtained with the Infrared Spectrometer and Array Camera (ISAAC, see Moorwood et al. 1999) installed at the first Unit Telescope (named Antu) of the ESO-VLT located in Cerro Paranal, Chile. The data were taken with the medium resolution grating and the narrowest available slit (0.3 arcsec), providing a spectral resolution of about 8000. In total, 19 settings of the grating were used to cover the range 0.997 – 2.25 μm. This wavelength range was scanned using the grating at different orders, with the corresponding order sorting filters (see Table 1). Some regions are missing at $\sim 1.4\mu m$ and $\sim 1.9\mu m$ corresponding to regions of high atmospheric absorption between the J and H and H and K atmospheric windows respectively and / or regions of non-overlapping transmission of the order sorting filters (see the on-line ISAAC User Manual for a plot of the filter transmission curves superimposed to the atmospheric transmission spectrum at http://www.eso.org/instruments/isaac).

For each grating setting, the wavelength scale was calibrated by using the OH lines themselves. Between 5 and 47 lines were used to determine the wavelength scale and the fit residual varied between 0.03 and 0.113 Å. Table 1 presents the details. The spectra have not been corrected for atmospheric absorption, which is mainly caused by water, nor have they been corrected for instrument throughput, which is a function of the grating efficiency curve, the transmission of the order sorting filter, instrument and telescope optics and, lastly, the detector. Indeed, one should be wary of using these data to compare line ratios. The continuum appearing between the OH lines is several order of magnitude fainter than the OH lines themselves.
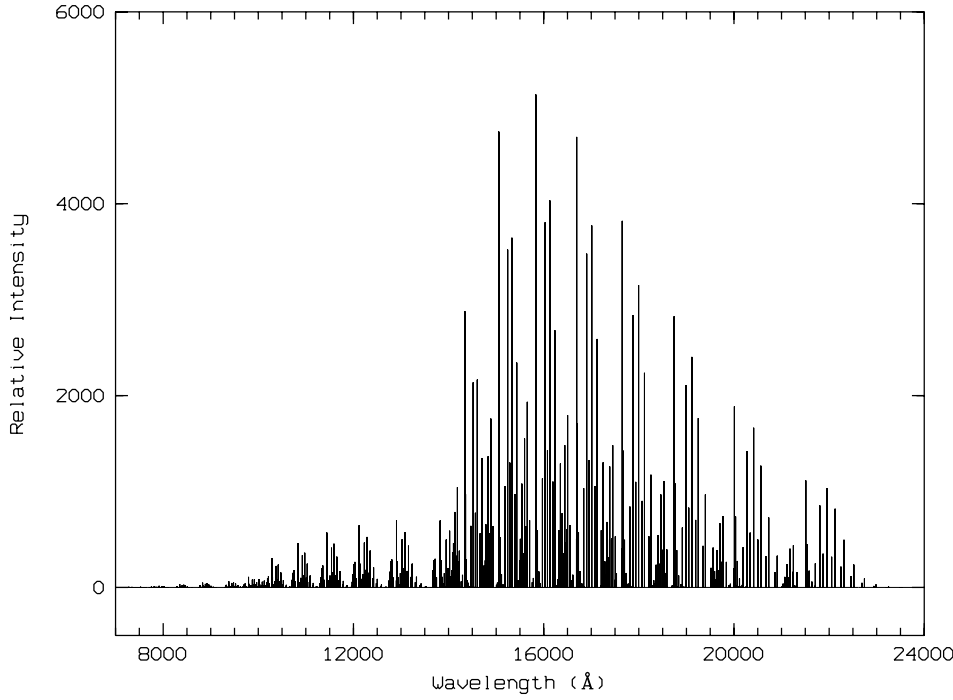
Fig. 1. General synthetic spectrum of the night-sky OH emission. This spectrum has been computed by using the code described in the part 3 of this paper. The relative intensities are proportional to the photon fluxes.

Table 1. Details of the wavelength calibration for each spectrum published in this paper.

Filter	Central wavelength (μm)	Airmass	Number of OH lines used	Wavelength dispersion (μm)	Fit residual (Å)
SZ filter	1.02	1.52	29	0.466	0.038
(5th order)	1.06	1.48	17	0.459	0.030
J filter	1.11	1.13	16	0.609	0.034
(4th order)	1.14	1.12	14	0.604	0.043
	1.19	1.10	19	0.597	0.032
	1.24	1.09	34	0.588	0.050
	1.29	1.08	47	0.579	0.068
	1.34	1.07	5	0.576	0.113
SH filter	1.41	1.22	10	0.824	0.028
(3rd order)	1.44	1.21	16	0.817	0.067
	1.52	1.19	22	0.806	0.046
	1.58	1.18	20	0.796	0.037
	1.65	1.16	17	0.785	0.039
	1.72	1.14	16	0.772	0.031
	1.79	1.13	9	0.761	0.054
SK filter	1.89	1.28	6	1.260	0.065
(2nd order)	1.99	1.30	18	1.249	0.071
	2.09	1.32	20	1.236	0.056
	2.19	1.34	14	1.222	0.056

3. Theoretical OH line identification

Fig. 2 represents the energy level diagram corresponding to the OH levels responsible for the infrared lines appearing in the sky. The electronic state involved by these lines is the ground state, called $X^2\Pi_i$. This state is constituted by two sub-states called $X^2\Pi_{1/2}$ and $X^2\Pi_{3/2}$. This multiplet structure, commonly known as spin-splitting, is due to the interaction between the electron spin vector and the orbital angular momentum vector along the internuclear axis. Because this ground state is inverted, the energy levels of the states $X^2\Pi_{3/2}$ are lower than the energy levels of the state $X^2\Pi_{1/2}$.

The angular momentum K can be used for numbering the rotational states. With this nomenclature the total angular momentum J (which takes into account the electronic spin) is equal to K+1/2 in the state $X^2\Pi_{3/2}$ and, in a same manner, J=K-1/2 in the state $X^2\Pi_{1/2}$. Each Λ-doublet has a "+" or a "-" subscript, depending on the parity of the electronic wave functions to reflection in a plane through the internuclear axis. Each lower doublet is labelled "e" and each upper doublet is labelled "f".
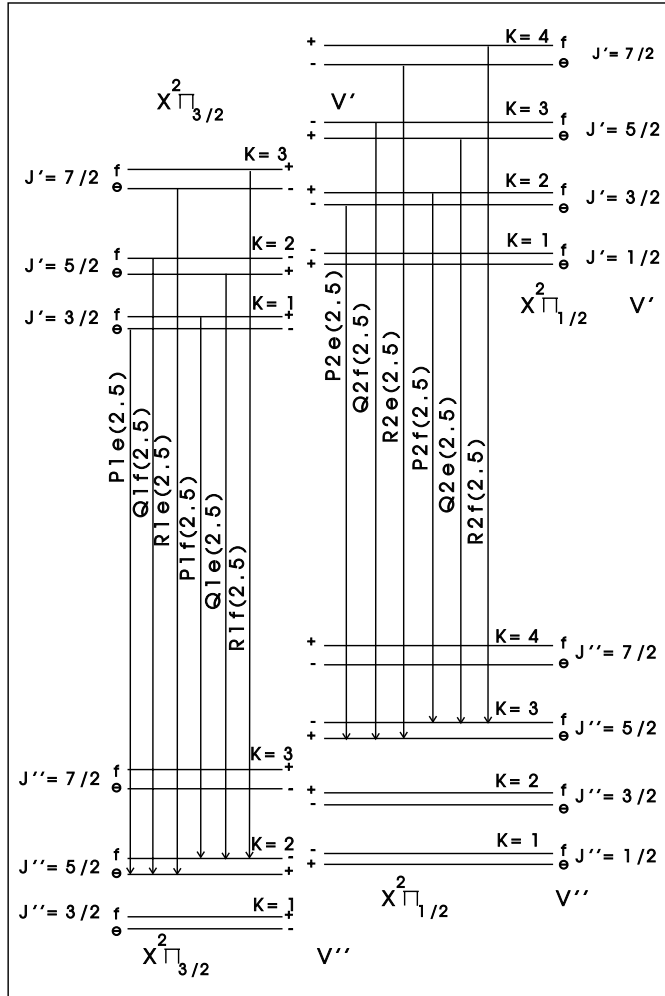
Fig. 2. Energy levels involved in the infrared rotation-vibration bands of the OH molecule.

The notations used in the Fig. 2 are those commonly accepted. The letters Q refer to the transitions with J'=J" (where ' refers to the upper state and " to the lower state), P to the transitions with J'=J"-1 and R to the transitions with J'=J"+1. The subscript 1 or 2 refers to the sub-state involved ($X^2\Pi_{3/2}$ or $X^2\Pi_{1/2}$). The number in parenthesis indicates the value of J" involved and the subscript "e" or "f" to the kind of doublet from which the line comes from (i.e. the upper state). Because the selection rules imply that symmetric levels interact only with antisymmetric levels (i.e. "+" with "-") and antisymmetric levels with symmetric levels, it can be seen that "e" levels interact with "e" levels for the P and R lines and "f" for Q lines, and that "f" levels interact with "f" levels for the P and R lines and "e" levels for the Q lines.

In Fig. 2 the satellite transitions, i.e. the transitions implying simultaneously the $X^2\Pi_{3/2}$ and $X^2\Pi_{1/2}$ states, are not shown. Indeed their probability of transitions are very low and they have not been considered in our work.

The identification of the OH lines in the observational spectra was conducted thanks to our code based both on laboratory data for the energy levels and on theoretical calculations for the probability of transitions. The energy levels have been taken from Abrams et al. (1994). All the levels having J≤16.5 have been taken into account. The resulting wavelengths obtained by using these values can be considered secure to about one hundredth of Angstrom.

The relative intensities have been computed by assuming a Boltzmann distribution for the upper relative population levels. Two different excitation temperatures have been used. The first one is the rotational temperature, which is very close to the kinetic temperature of the gas in which the OH lines are formed, i.e. about 200 K. The second one is the vibrational temperature. Because of the initial energy contained by the OH radicals just after their creation and the different relaxation time, the vibrational temperature does not correspond to the kinetic temperature. Wallace (1962, 1968) explains that the vibrational temperature would be much higher than the rotational temperature, with a value between 8500 and 13000 K.

In our calculations we used $T_{rot} = 190$ K and $T_{vib} = 9000$ K. The purpose of these calculations is to identify without ambiguities the observational lines; the accuracy of these values is not critical. The intensities have been computed using the transition of probabilities published by Mies (1974). These transition probabilities result from theoretical calculations and do not distinguish between the two lambda-components. The intensities of these two components have been considered equal.

4. Atlas

Figs. 3 to 23 show the Cerro Paranal night-sky spectra as observed with ISAAC for each grating position from 9970 to 22500 Å with line identifications and wavelengths given in vacuum. The intensities are relative within each plot, normalized to 1.

Since the two components of the lambda-doublets have equal intensities and are usually not resolved in our observations, the corresponding wavelengths reported on the figures are the arithmetic means of the wavelengths of the two components. The line identification therefore omits the reference to the "e" or "f" components, except whenever the separation between the two components exceeds 1 Å, in which case both lines are identified.
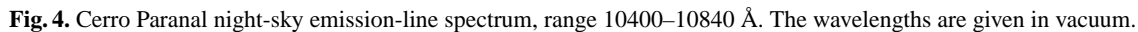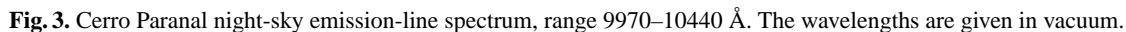
Some OH lines computed theoretically appear to be completely missing in the observational data. This is due to atmospheric absorption located below the OH layer, and also to the order sorting filters. The most affected regions are around 1.4 μm and 1.9 μm, where atmospheric water vapor exhibits strong absorption bands (Wyatt et al. 1964). Where these lines do not appear at all, they were not included in the figures.

In addition to OH emission, the J band also exhibits strong O_2 emission lines which have been identified. The detail of the identification of these lines is shown in Fig. 9 and 11, with the corresponding wavelengths in Table 2. They correspond to the (0,0) band of the $a^1\Delta_g - X^3\Sigma_g^-$ transition in the O_2 molecule. The vacuum wavenumbers are taken from Herzberg & Herzberg (1947). They had identified these lines by using the solar spectrum and the vacuum wave numbers for most of the lines appearing in the ISAAC spectra are given in their Table 1.

Table 2. Wavelengths of the O_2 lines. They are expressed in Angstroems, in vacuum, with the corresponding air wavelength below, inside the parenthesis.

J"	$^S R$	$^R R$	$^R Q$	$^Q Q$	$^Q P/^Q R$[1]	$^P P$	$^P Q$	$^O P$
1		12677.36 (12673.89)						
2	12660.65 (12657.19)		12674.33 (12670.86)		12683.54 (12680.07)		12697.25 (12693.77)	
3		12668.59 (12665.13)		12686.76 (12683.29)		12700.56 (12697.09)		
4	12642.64 (12639.18)		12665.46 (12662.00)		12684.12 (12680.65)		12707.00 (12703.53)	12725.37 (12721.89)
5		12660.02 (12656.56)		12687.23 (12683.76)		12710.25 (12706.77)		
6	12625.24 (12621.78)		12656.85 (12653.39)		12684.97 (12681.50)		12717.08 (12713.60)	12744.68 (12741.19)
7		12651.88 (12648.42)		12688.13 (12684.66)		12720.26 (12716.78)		
8	12607.97 (12604.53)		12648.59 (12645.13)		12686.10 (12682.64)		12727.11 (12723.63)	12764.18 (12760.69)
9		12643.88 (12640.42)		12689.24 (12685.77)		12730.49 (12727.01)		
10	12590.96 (12587.52)		12640.59 (12637.13)		12687.23 (12683.76)		12737.98 (12734.49)	12784.15 (12780.66)
11		12636.82 (12633.36)		12690.76 (12687.29)		12741.04 (12737.56)		
12	12574.34 (12570.91)		12632.82 (12629.37)		12689.24 (12685.77)		12748.73 (12745.24)	12804.20 (12800.70)
13		12628.73 (12625.28)		12692.43 (12688.95)		12751.88 (12748.40)		
14	12558.05 (12554.61)		12625.24 (12621.78)		12690.76 (12687.29)		12759.93 (12756.44)	12824.73 (12821.22)
15		12621.55 (12618.10)		12694.12 (12690.65)		12762.90 (12759.41)		
16	12542.02 (12538.59)		12618.21 (12614.76)		12692.98 (12689.50)		12771.13 (12767.63)	12845.51 (12842.00)
17		12614.65 (12611.20)		12696.19 (12692.72)		12774.35 (12770.86)		
18	12526.43 (12523.00)		12611.27 (12607.83)		12695.59 (12692.12)		12782.85 (12779.35)	12866.57 (12863.05)
19		12607.98 (12604.53)		12698.60 (12695.13)		12785.87 (12782.37)		
20	12510.97 (12507.55)		12604.71 (12601.27)		12697.95 (12694.48)		12794.68 (12791.18)	12888.08 (12884.55)
21		12601.77 (12598.33)		12701.43 (12697.96)		12797.67 (12794.17)		
22	12495.99 (12492.57)		12598.44 (12594.99)		12700.92 (12697.44)		12806.96 (12803.46)	12909.63 (12906.10)
23		12595.66 (12592.21)		12704.22 (12700.74)		12809.94 (12806.43)		
24	12481.37 (12477.95)		12592.20 (12588.76)		12704.50 (12701.03)		12819.35 (12815.85)	12931.74 (12928.20)
25						12822.28 (12818.78)		
26								12954.14 (12950.60)

[1] J" refers to the $^Q P$ lines

Fig. 3. Cerro Paranal night-sky emission-line spectrum, range 9970–10440 Å. The wavelengths are given in vacuum.

Fig. 4. Cerro Paranal night-sky emission-line spectrum, range 10400–10840 Å. The wavelengths are given in vacuum.
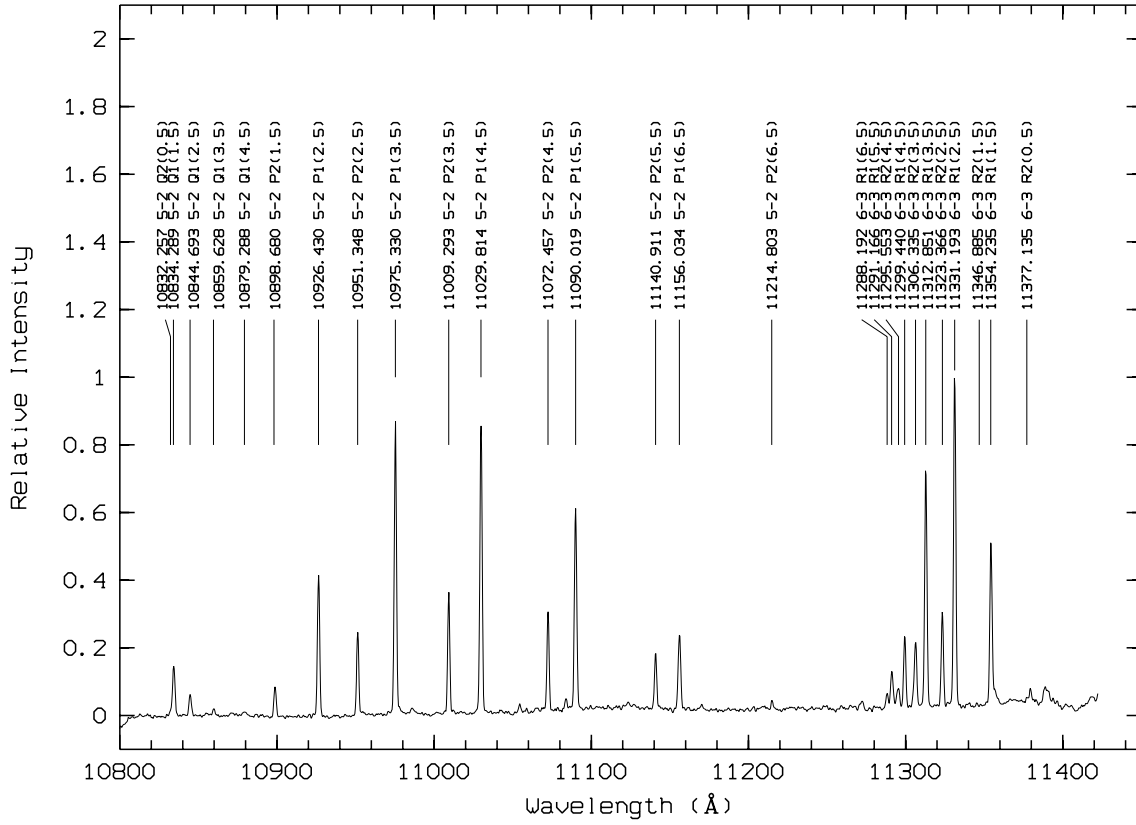
Fig. 5. Cerro Paranal night-sky emission-line spectrum, range 10800–11420 Å. The wavelengths are given in vacuum.
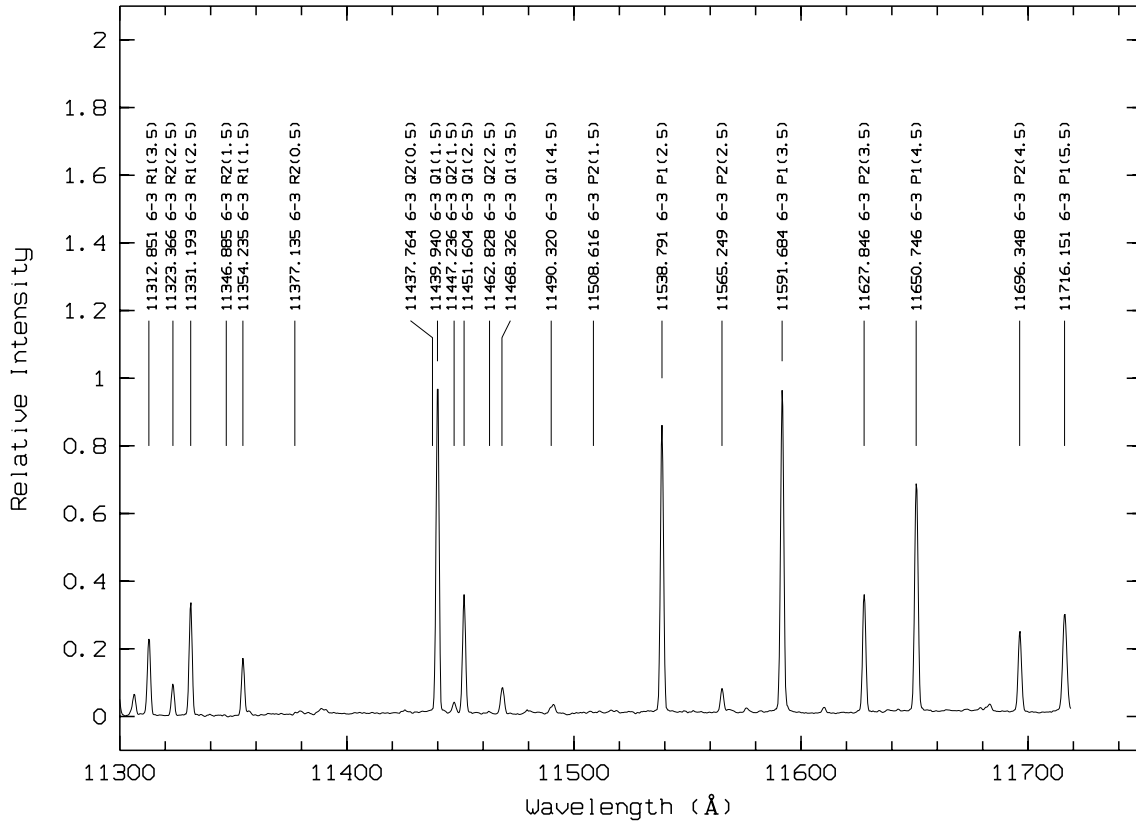

Fig. 6. Cerro Paranal night-sky emission-line spectrum, range 11300–11720 Å. The wavelengths are given in vacuum.
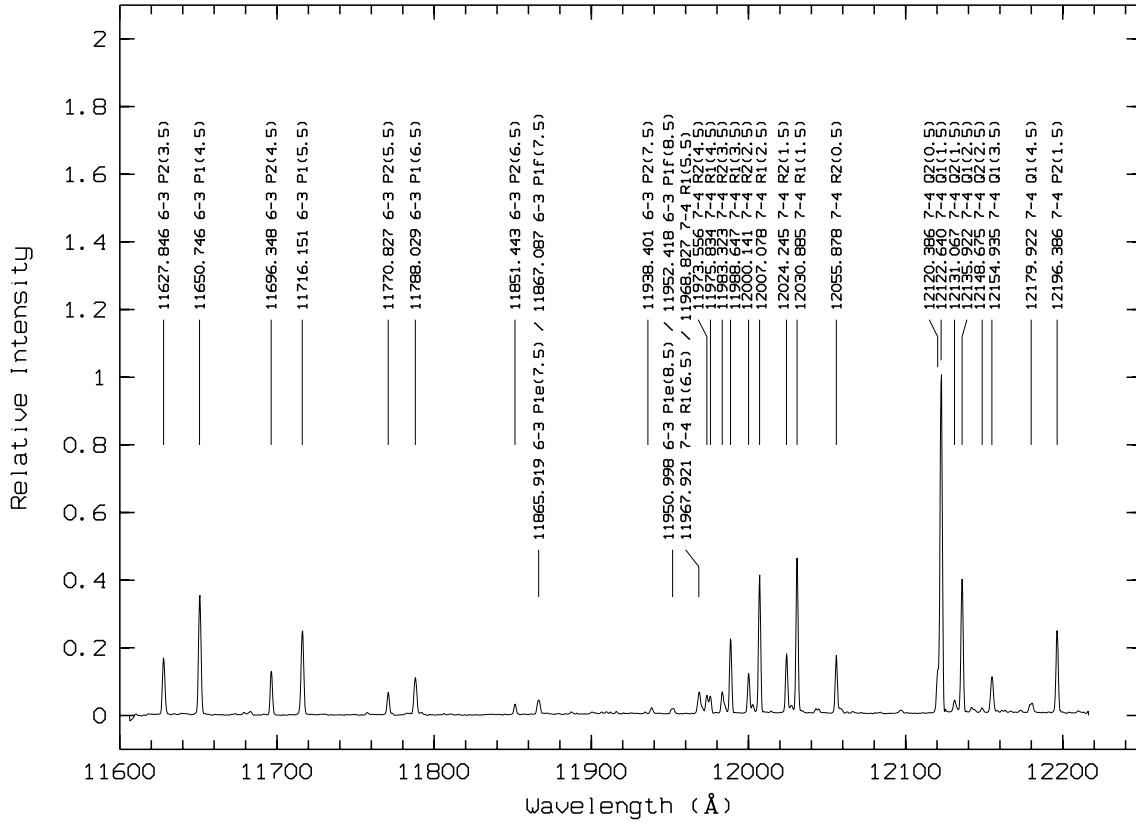
Fig. 7. Cerro Paranal night-sky emission-line spectrum, range 11600–12220 Å. The wavelengths are given in vacuum.
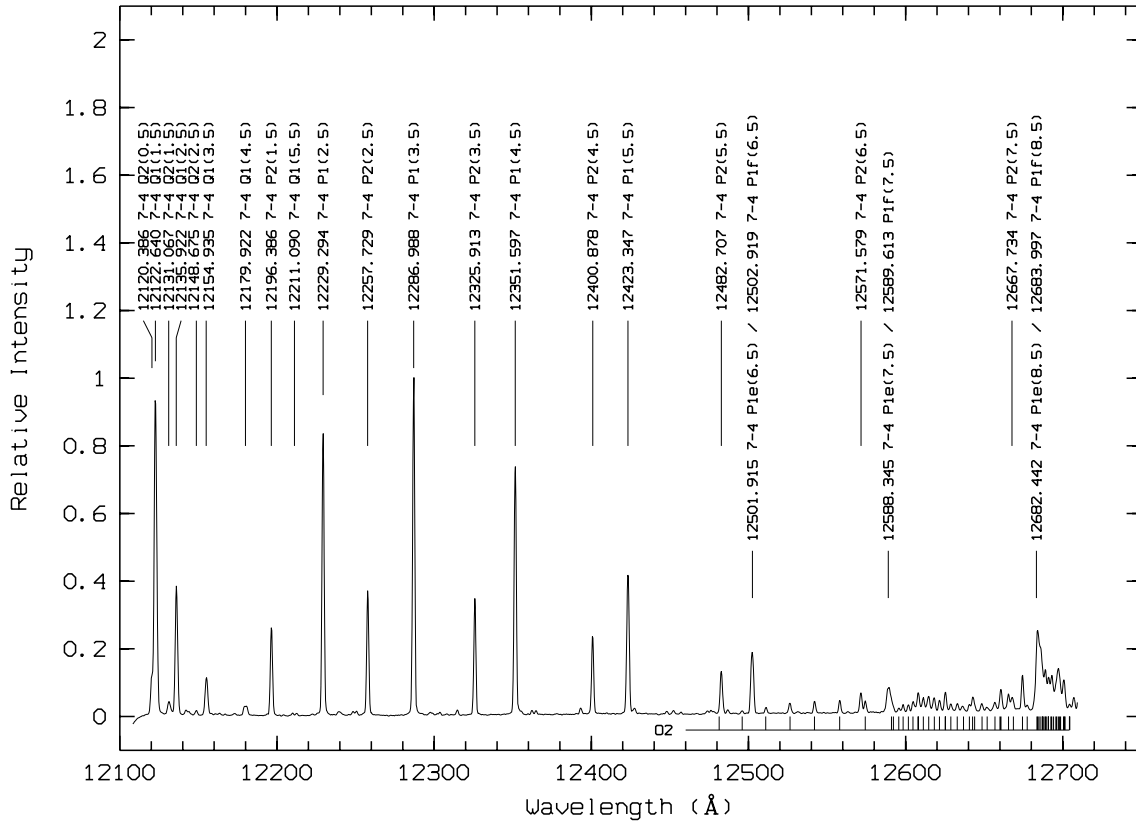

Fig. 8. Cerro Paranal night-sky emission-line spectrum, range 12100–12710 Å. The wavelengths are given in vacuum.
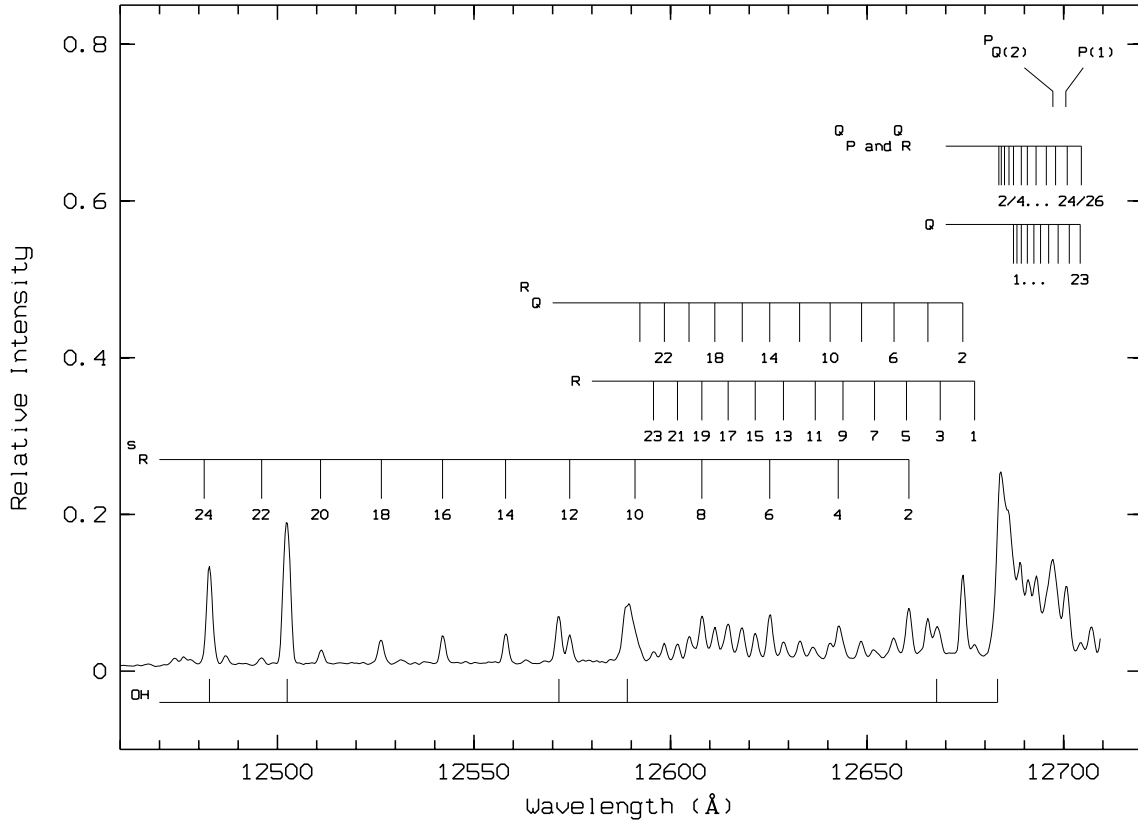
Fig. 9. Detail of the identification of the O_2 lines appearing in the Fig. 8
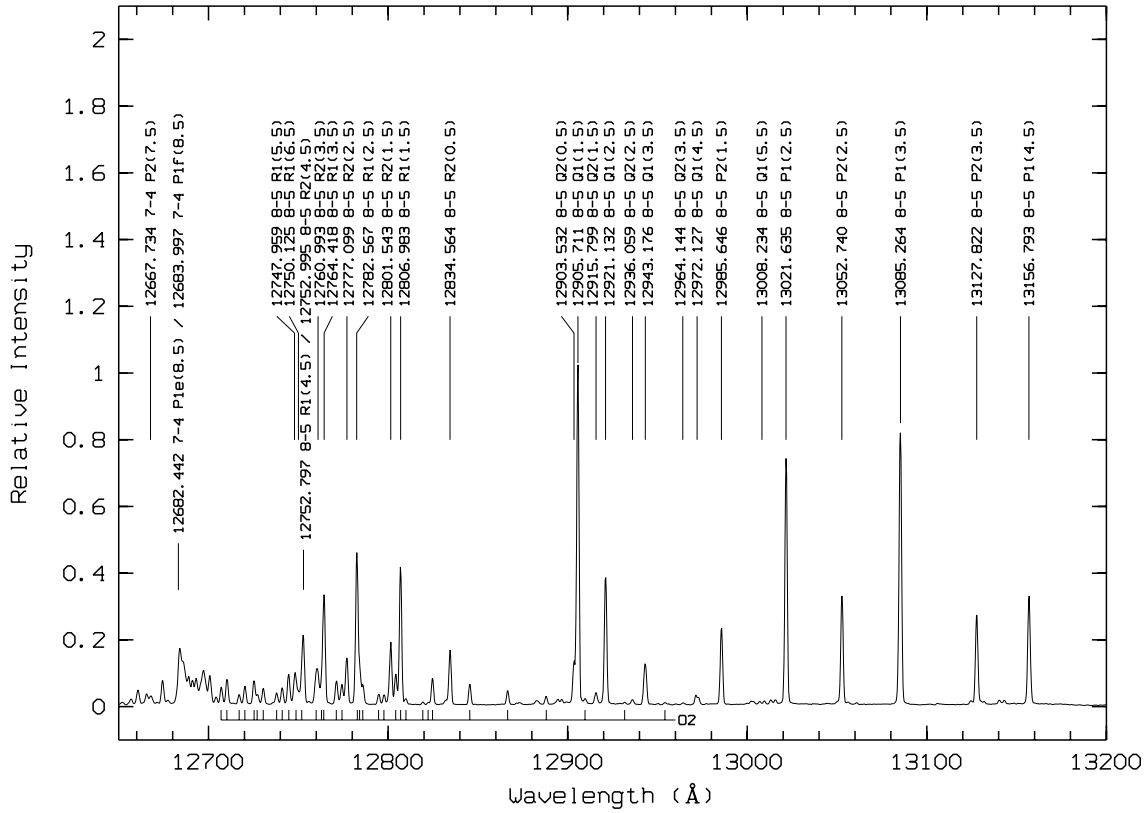

Fig. 10. Cerro Paranal night-sky emission-line spectrum, range 12650–13200 Å. The wavelengths are given in vacuum.

Fig. 11. Detail of the identification of the O$_2$ lines appearing in the Fig. 10

Fig. 12. Cerro Paranal night-sky emission-line spectrum, range 13100–13700 Å. The wavelengths are given in vacuum.
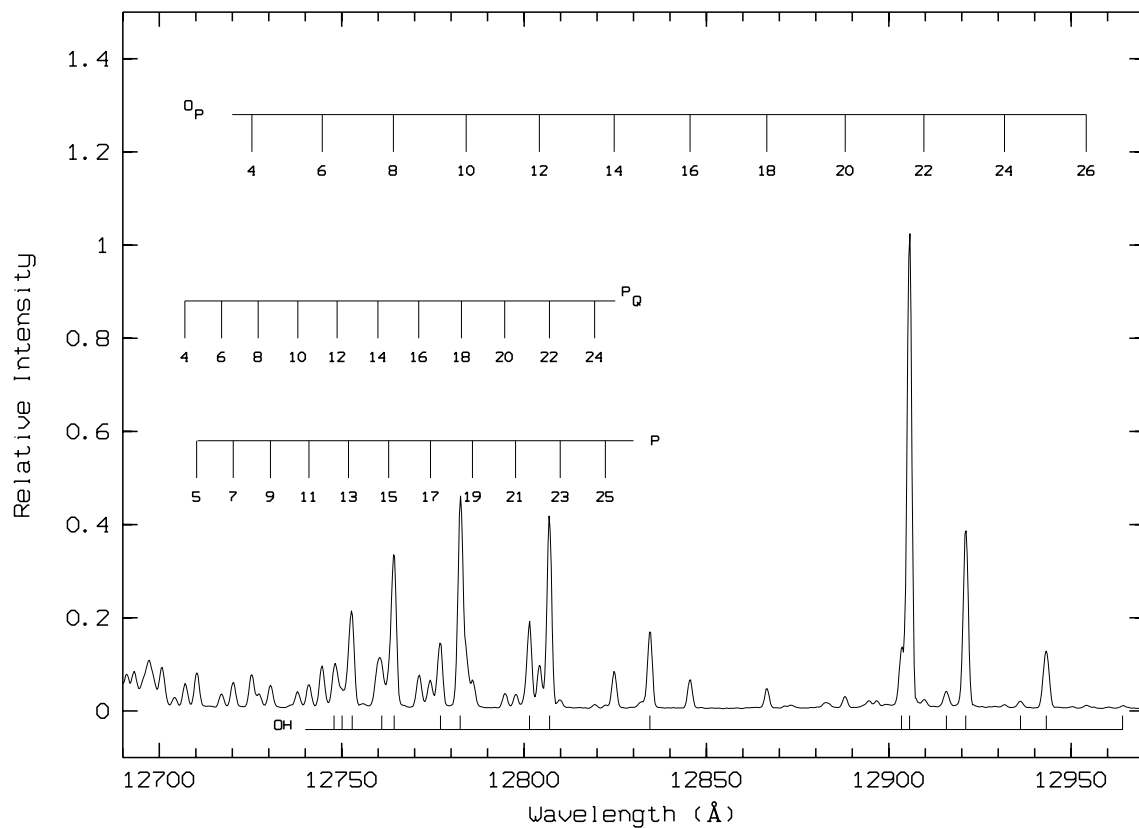
Fig. 13. Cerro Paranal night-sky emission-line spectrum, range 13700–14550 Å. The wavelengths are given in vacuum.
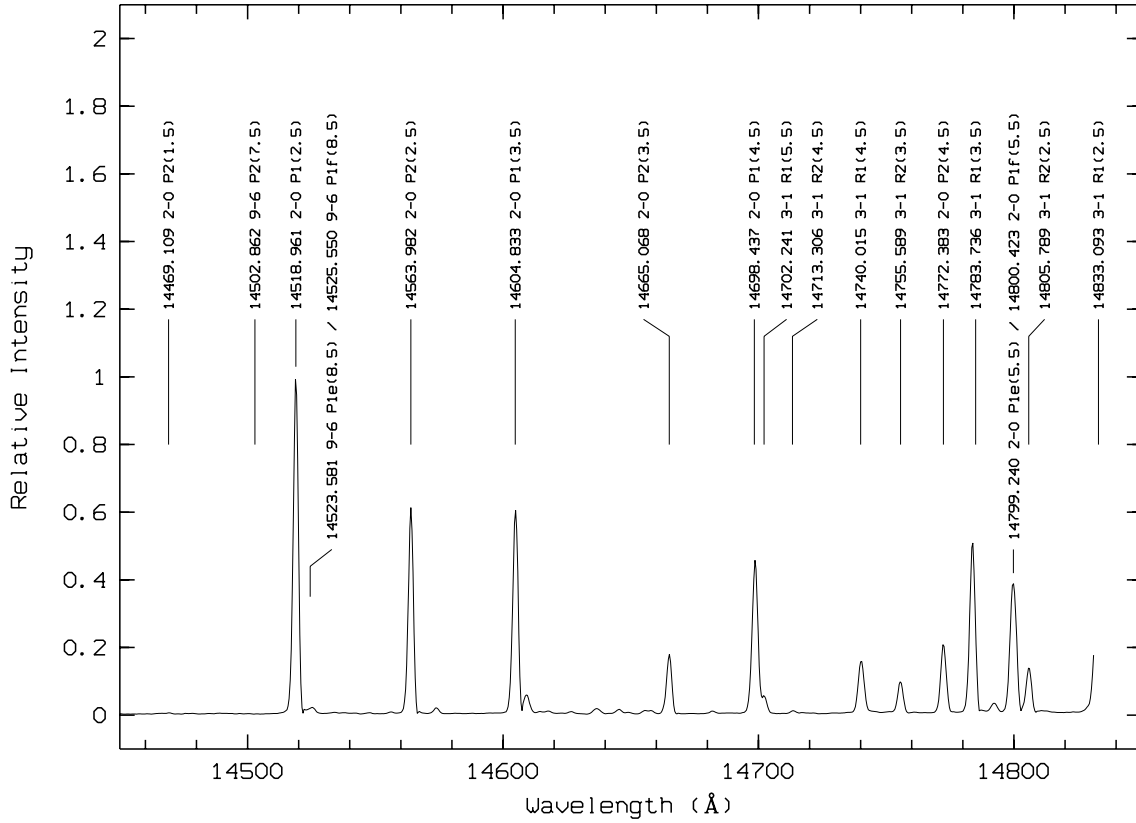
Fig. 14. Cerro Paranal night-sky emission-line spectrum, range 14350–14830 Å. The wavelengths are given in vacuum.

Fig. 15. Cerro Paranal night-sky emission-line spectrum, range 14800–15620 Å. The wavelengths are given in vacuum.

Fig. 16. Cerro Paranal night-sky emission-line spectrum, range 15400–16220 Å. The wavelengths are given in vacuum.
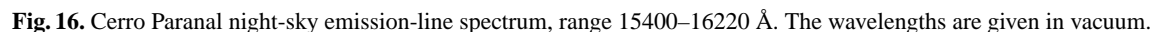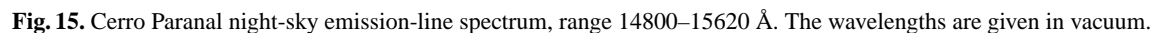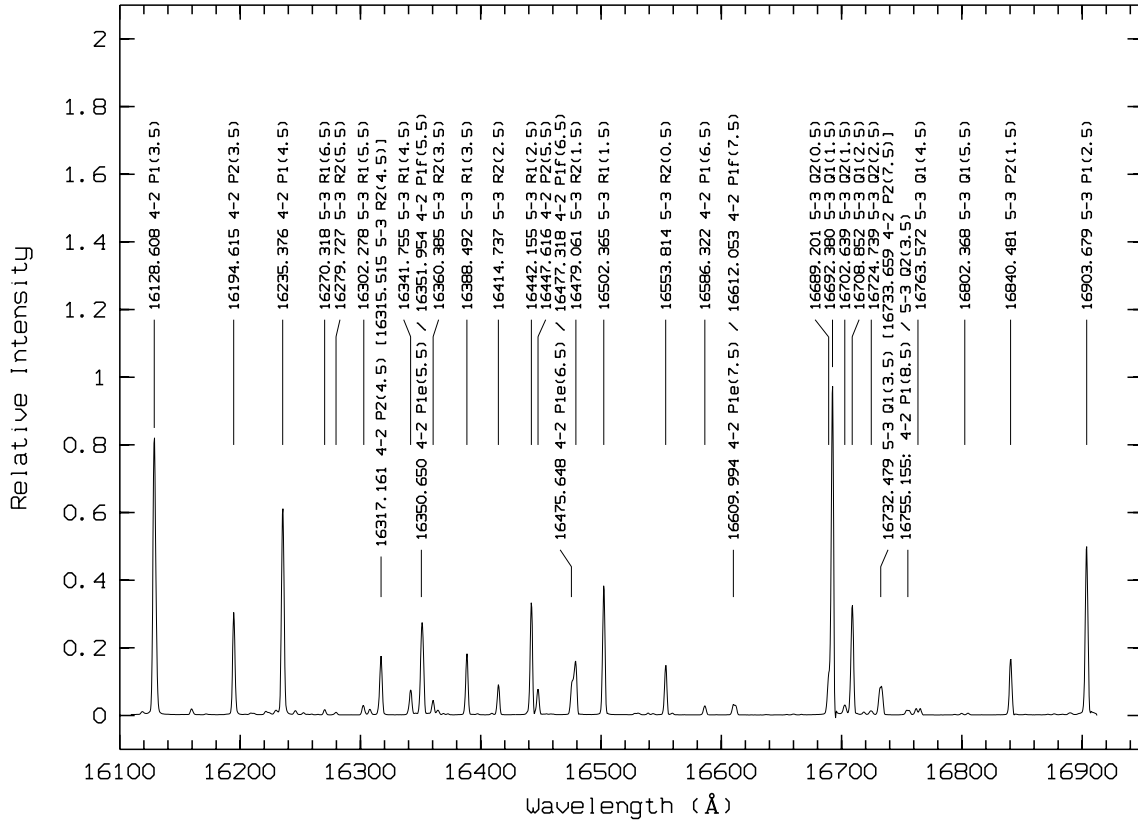
Fig. 17. Cerro Paranal night-sky emission-line spectrum, range 16110–16910 Å. The wavelengths are given in vacuum.
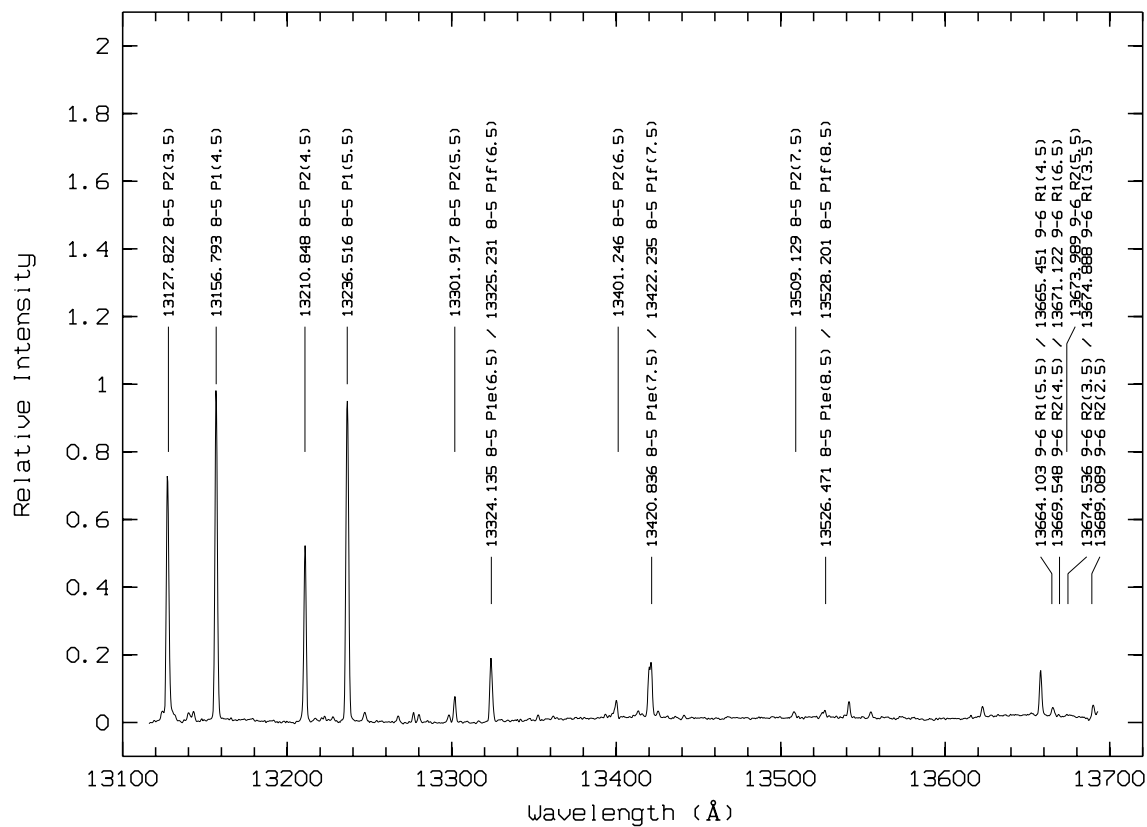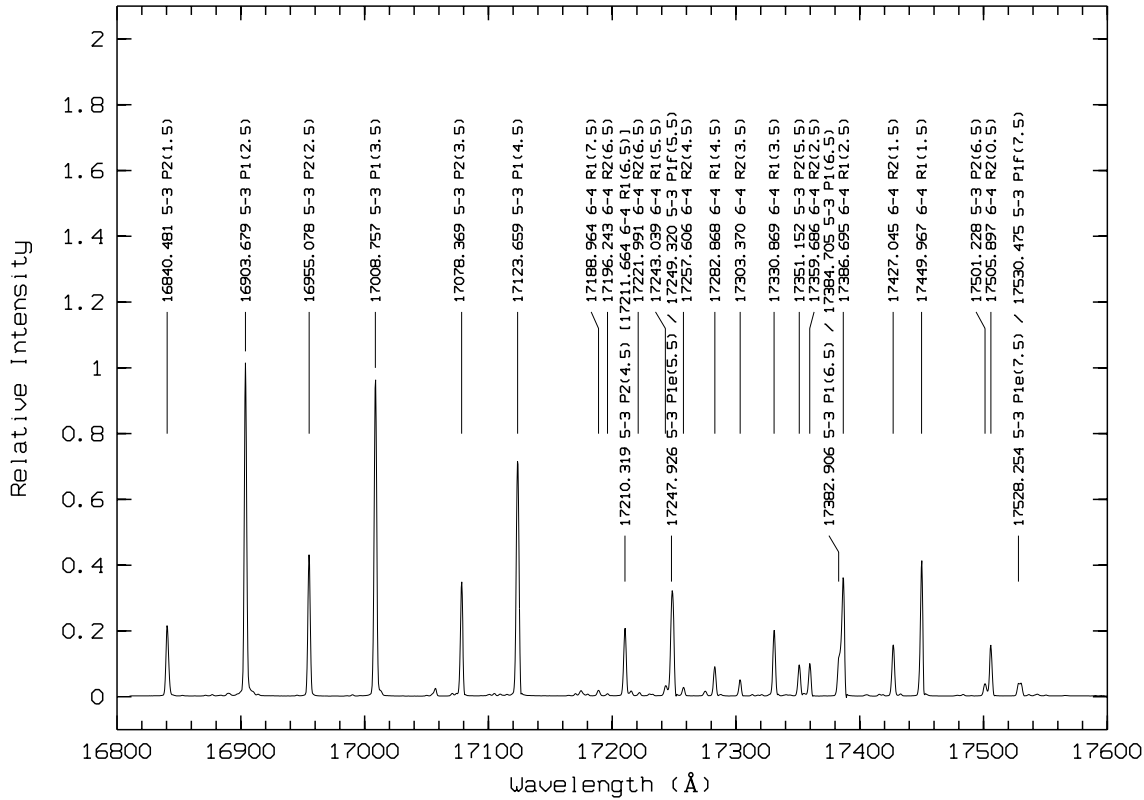

Fig. 18. Cerro Paranal night-sky emission-line spectrum, range 16800–17600 Å. The wavelengths are given in vacuum.
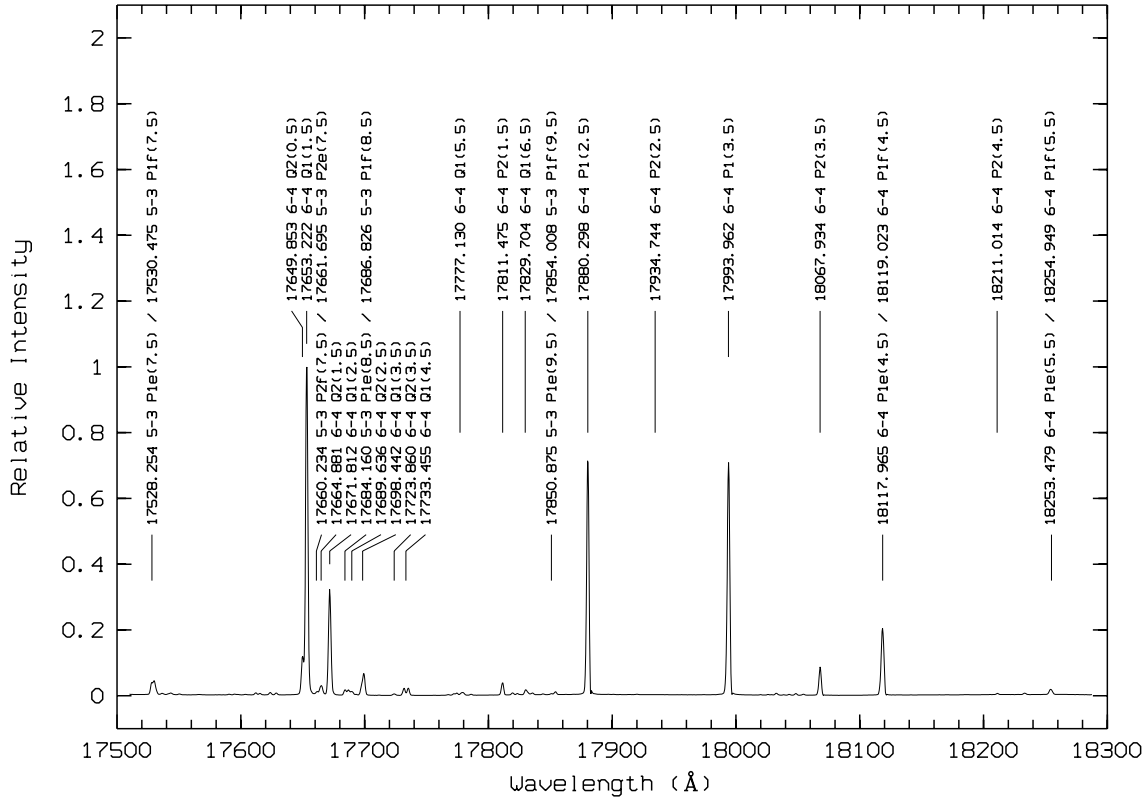
Fig. 19. Cerro Paranal night-sky emission-line spectrum, range 17500–18300 Å. The wavelengths are given in vacuum.
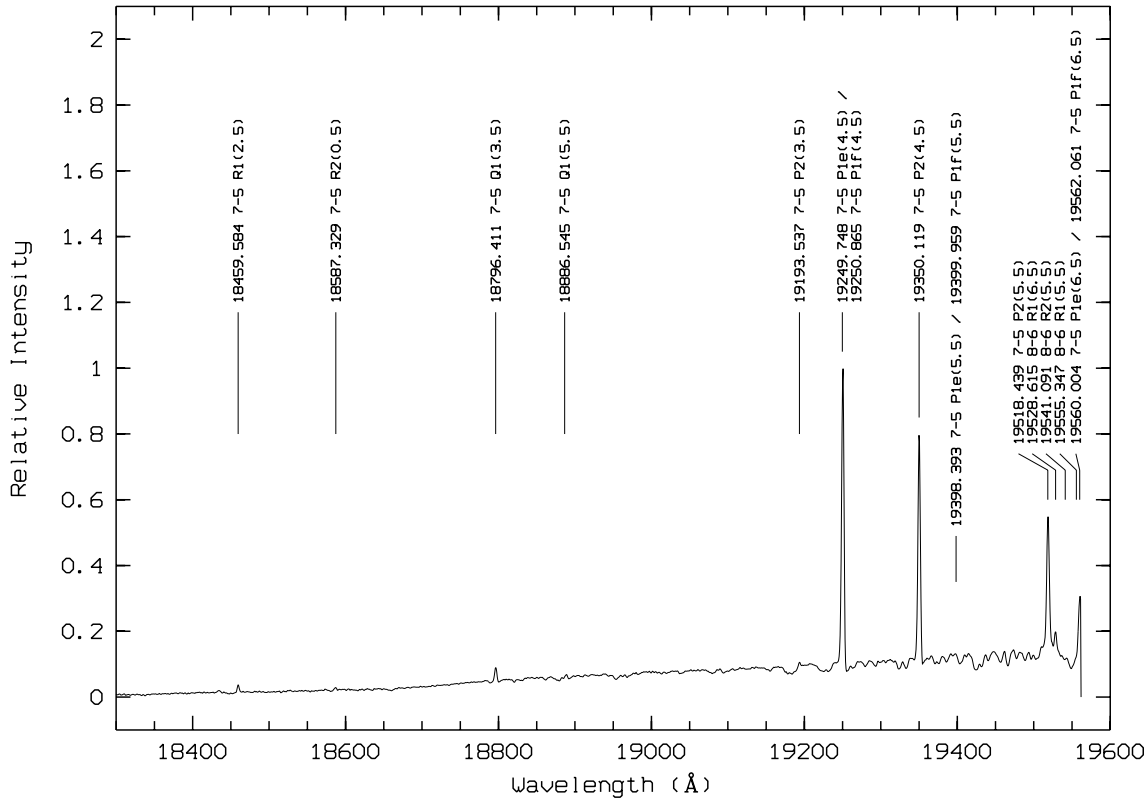
Fig. 20. Cerro Paranal night-sky emission-line spectrum, range 18300–19560 Å. The wavelengths are given in vacuum.
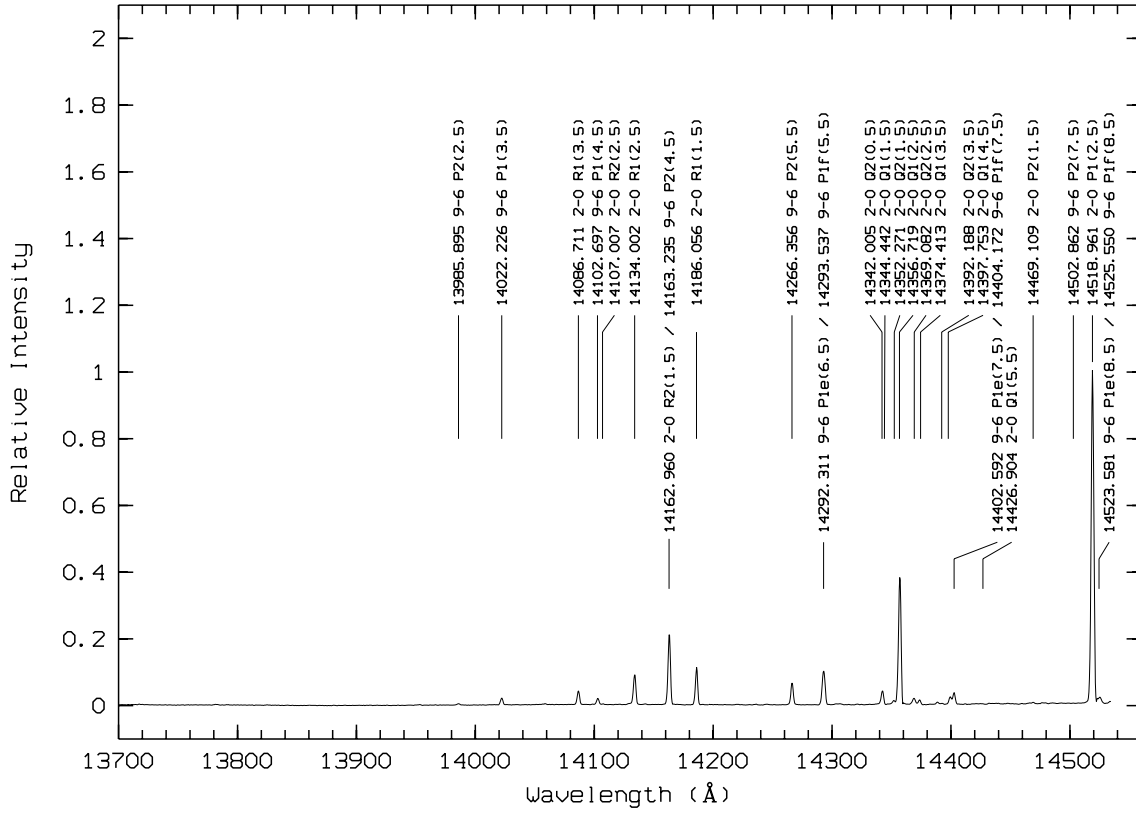
Fig. 21. Cerro Paranal night-sky emission-line spectrum, range 19300–20560 Å. The wavelengths are given in vacuum.

Fig. 22. Cerro Paranal night-sky emission-line spectrum, range 20400–21550 Å. The wavelengths are given in vacuum.

Fig. 23. Cerro Paranal night-sky emission-line spectrum, range 21400–22550 Å. The wavelengths are given in vacuum.
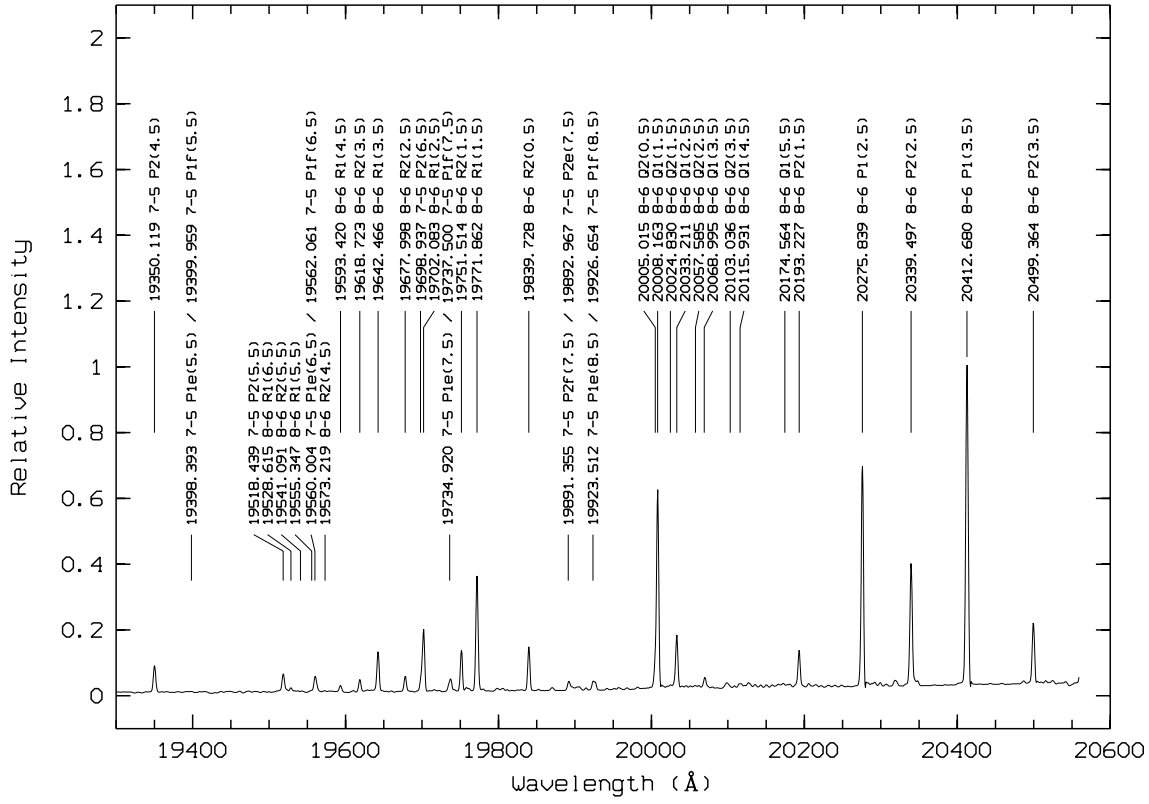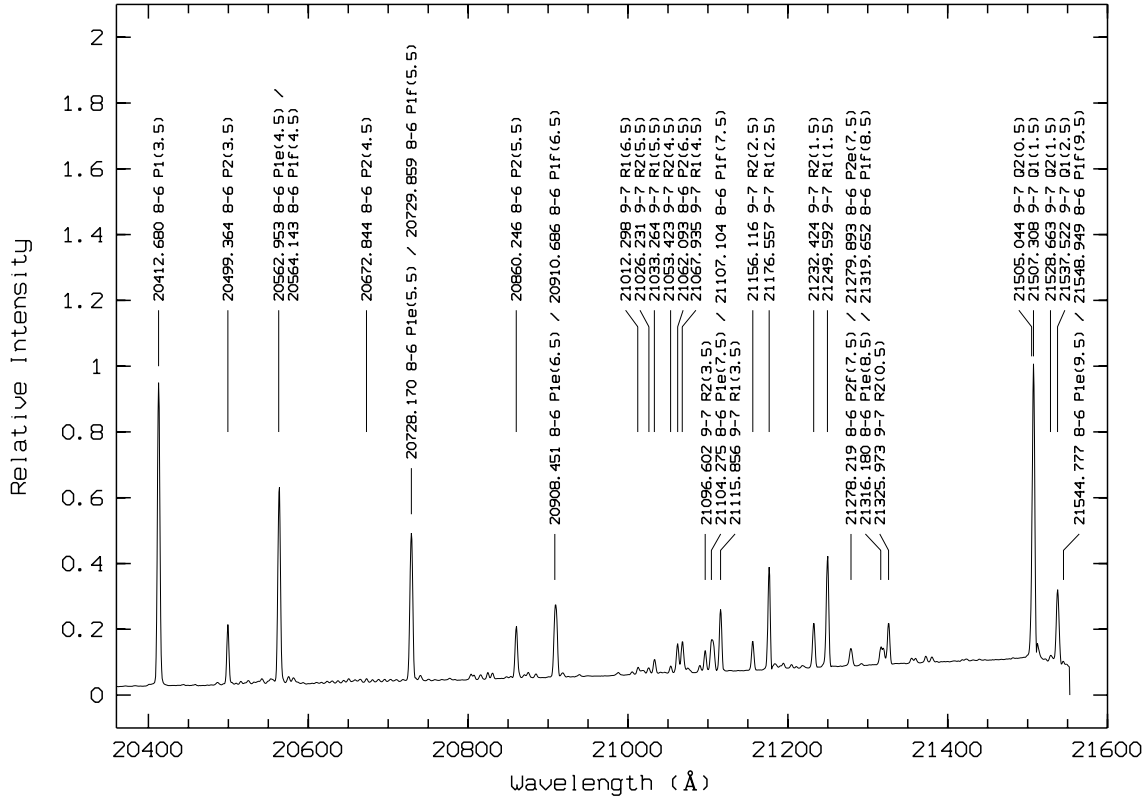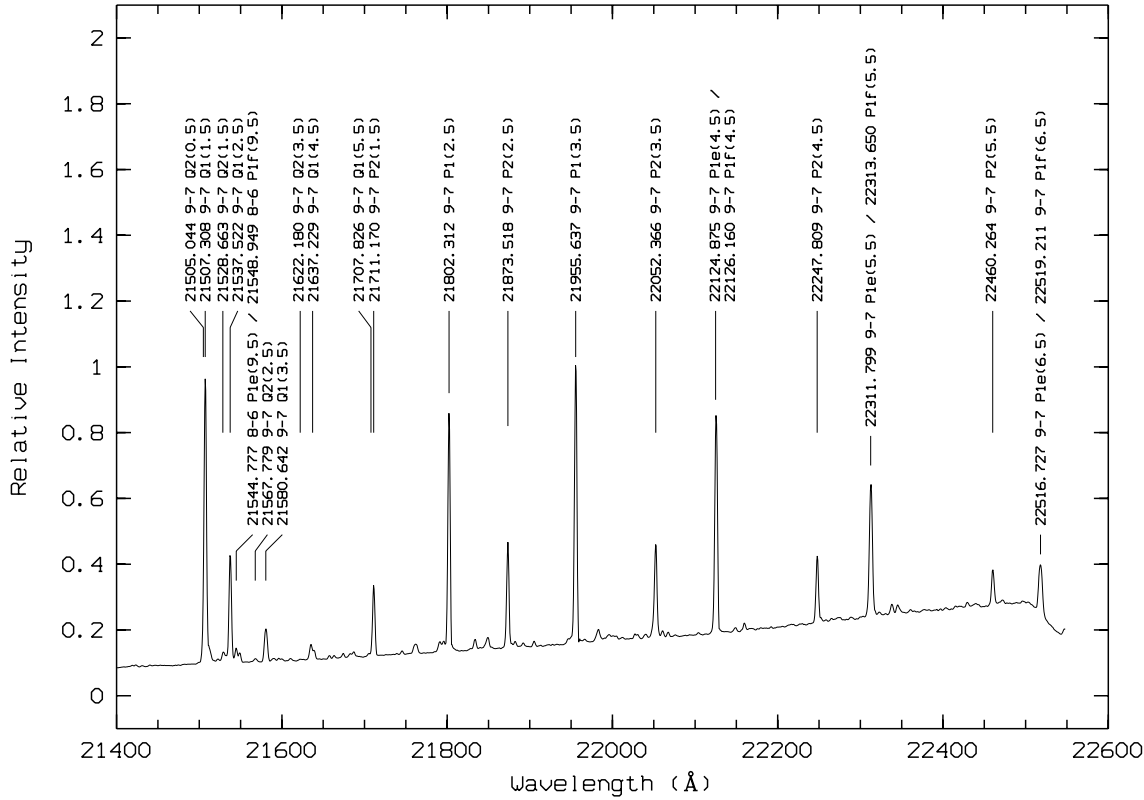
Table 3. Conversion of the vacuum wavelengths to air wavelengths.

λ_{vac}	λ_{air}	λ_{vac}	λ_{air}	λ_{vac}	λ_{air}	λ_{vac}	λ_{air}	λ_{vac}	λ_{air}
9975.083	9972.349	10192.499	10189.706	10575.401	10572.504	11029.814	11026.794	11591.684	11588.512
10002.737	9999.996	10205.844	10203.047	10588.762	10585.862	11072.457	11069.426	11627.846	11624.664
10014.086	10011.341	10211.576	10208.778	10643.675	10640.760	11090.019	11086.983	11650.746	11647.558
10015.555	10012.810	10213.851	10211.052	10654.707	10651.789	11140.911	11137.861	11696.348	11693.147
10016.731	10013.986	10211.576	10208.778	10655.706	10652.788	11156.034	11152.980	11716.151	11712.945
10024.084	10021.337	10228.586	10225.783	10686.683	10683.756	11214.803	11211.733	11770.827	11767.606
10028.200	10025.452	10233.464	10230.660	10689.208	10686.280	11288.192	11285.102	11788.029	11784.803
10046.266	10043.513	10273.897	10271.082	10690.996	10688.068	11291.166	11288.075	11851.443	11848.200
10061.781	10059.024	10287.588	10284.769	10695.088	10692.159	11295.553	11292.461	11865.919	11862.672
10063.472	10060.714	10289.457	10286.638	10700.044	10697.114	11299.440	11296.347	11867.087	11863.840
10069.986	10067.226	10295.345	10292.524	10706.408	10703.476	11306.335	11303.240	11938.401	11935.135
10073.640	10070.879	10298.845	10296.023	10713.680	10710.746	11312.851	11309.754	11950.998	11947.728
10085.231	10082.467	10308.075	10305.251	10723.350	10720.413	11323.366	11320.266	11952.418	11949.148
10106.374	10103.604	10312.344	10309.519	10731.714	10728.775	11331.193	11328.091	11967.921	11964.647
10126.784	10124.009	10330.129	10327.299	10746.152	10743.209	11346.885	11343.779	11968.827	11965.552
10135.225	10132.448	10342.865	10340.031	10753.920	10750.975	11354.235	11351.127	11973.556	11970.280
10135.424	10132.647	10350.127	10347.291	10775.059	10772.108	11377.135	11374.021	11975.834	11972.557
10146.587	10143.807	10356.827	10353.990	10832.257	10829.291	11437.764	11434.633	11983.323	11980.044
10148.995	10146.214	10375.720	10372.877	10834.289	10831.322	11439.940	11436.809	11988.647	11985.367
10151.784	10149.002	10399.386	10396.537	10844.693	10841.723	11447.236	11444.103	12000.141	11996.858
10155.610	10152.827	10421.218	10418.363	10859.628	10856.654	11451.604	11448.470	12007.078	12003.793
10155.755	10152.972	10430.798	10427.941	10879.288	10876.309	11462.828	11459.691	12024.245	12020.955
10161.266	10158.482	10432.012	10429.154	10898.680	10895.696	11468.326	11465.187	12030.885	12027.593
10167.160	10164.374	10453.365	10450.501	10926.430	10923.438	11490.320	11487.175	12055.878	12052.580
10174.488	10171.700	10471.830	10468.961	10951.348	10948.349	11508.616	11505.466	12120.386	12117.070
10174.898	10172.110	10512.011	10509.132	10975.330	10972.325	11538.791	11535.633	12122.640	12119.324
10183.825	10181.034	10527.657	10524.773	11009.293	11006.279	11565.249	11562.084	12131.067	12127.748

Table 3. (continued)

λ_{vac}	λ_{air}	λ_{vac}	λ_{air}	λ_{vac}	λ_{air}	λ_{vac}	λ_{air}	λ_{vac}	λ_{air}
12135.922	12132.602	13526.471	13522.773	14931.883	14927.803	16317.161	16312.705	17661.695	17656.873
12148.675	12145.351	13528.201	13524.503	15006.737	15002.637	16341.755	16337.292	17664.881	17660.058
12154.935	12151.610	13664.103	13660.368	15025.143	15021.038	16350.650	16346.185	17671.812	17666.987
12179.922	12176.590	13665.451	13661.716	15026.969	15022.864	16351.954	16347.488	17684.160	17679.332
12196.386	12193.050	13669.548	13665.811	15052.866	15048.753	16360.385	16355.917	17686.826	17681.997
12211.090	12207.750	13671.122	13667.385	15055.550	15051.437	16388.492	16384.016	17689.636	17684.806
12229.294	12225.949	13673.989	13670.251	15063.998	15059.882	16414.737	16410.254	17698.442	17693.610
12257.729	12254.376	13674.536	13670.798	15068.968	15064.851	16442.155	16437.665	17723.860	17719.021
12286.988	12283.627	13674.888	13671.150	15082.254	15078.133	16447.616	16443.124	17733.455	17728.614
12325.913	12322.541	13689.089	13685.347	15088.276	15084.154	16475.648	16471.149	17777.130	17772.277
12351.597	12348.218	13985.895	13982.072	15107.382	15103.255	16477.318	16472.818	17811.475	17806.612
12400.878	12397.486	14022.226	14018.394	15113.725	15109.596	16479.061	16474.561	17829.704	17824.836
12423.347	12419.949	14086.711	14082.861	15187.140	15182.991	16502.365	16497.858	17850.875	17846.002
12482.707	12479.293	14102.697	14098.843	15240.954	15236.790	16553.814	16549.293	17854.008	17849.134
12501.915	12498.496	14107.007	14103.152	15287.789	15283.613	16586.322	16581.793	17880.298	17875.417
12502.919	12499.499	14134.002	14130.139	15332.402	15328.213	16609.994	16605.458	17934.744	17929.848
12571.579	12568.141	14162.960	14159.089	15395.334	15391.128	16612.053	16607.517	17993.962	17989.050
12588.345	12584.902	14163.235	14159.364	15430.163	15425.948	16689.201	16684.644	18067.934	18063.002
12589.613	12586.170	14186.056	14182.179	15432.156	15427.940	16692.380	16687.822	18117.965	18113.019
12667.734	12664.270	14266.356	14262.457	15462.125	15457.901	16702.639	16698.078	18119.023	18114.077
12682.442	12678.974	14292.311	14288.405	15474.212	15469.985	16708.852	16704.289	18211.014	18206.043
12683.997	12680.528	14293.537	14289.631	15500.864	15496.630	16724.739	16720.172	18253.479	18248.496
12747.959	12744.473	14342.005	14338.086	15509.769	15505.532	16732.479	16727.910	18254.949	18249.966
12750.125	12746.638	14344.442	14340.522	15517.872	15513.633	16733.659	16729.089	18459.584	18454.545
12752.797	12749.309	14352.271	14348.349	15539.711	15535.466	16755.155	16750.580	18587.329	18582.255
12752.995	12749.507	14356.719	14352.796	15540.945	15536.700	16763.572	16758.994	18796.411	18791.280
12760.993	12757.503	14369.082	14365.155	15546.141	15541.894	16802.368	16797.780	18886.545	18881.390
12764.418	12760.927	14374.413	14370.485	15570.159	15565.906	16840.481	16835.882	19193.537	19188.298
12777.099	12773.605	14392.188	14388.255	15597.631	15593.370	16903.679	16899.063	19249.748	19244.494
12782.567	12779.071	14397.753	14393.819	15631.443	15627.173	16955.078	16950.448	19250.865	19245.611
12801.543	12798.042	14402.592	14398.656	15654.953	15650.677	17008.757	17004.113	19350.119	19344.838
12806.983	12803.481	14404.172	14400.236	15656.178	15651.901	17078.369	17073.706	19398.393	19393.099
12834.564	12831.054	14426.904	14422.962	15657.749	15653.472	17123.659	17118.983	19399.959	19394.664
12903.532	12900.004	14469.109	14465.155	15702.539	15698.250	17188.964	17184.271	19518.439	19513.112
12905.711	12902.182	14502.862	14498.899	15759.826	15755.521	17196.243	17191.548	19528.615	19523.285
12915.799	12912.267	14518.961	14514.994	15760.830	15756.525	17210.319	17205.620	19541.091	19535.758
12921.132	12917.599	14523.581	14519.612	15781.163	15776.852	17243.039	17238.331	19555.347	19550.010
12936.059	12932.522	14525.550	14521.581	15783.090	15778.779	17247.926	17243.217	19560.004	19554.666
12943.176	12939.637	14563.982	14560.002	15830.335	15826.011	17249.320	17244.610	19562.061	19556.722
12964.144	12960.599	14604.833	14600.842	15833.272	15828.947	17257.606	17252.894	19573.219	19567.877
12972.127	12968.580	14665.068	14661.061	15842.503	15838.176	17282.868	17278.149	19593.420	19588.072
12985.646	12982.095	14698.437	14694.421	15848.061	15843.732	17303.370	17298.646	19618.723	19613.369
13008.234	13004.677	14702.241	14698.224	15862.489	15858.156	17330.869	17326.137	19642.466	19637.105
13021.635	13018.074	14713.306	14709.286	15869.307	15864.973	17351.152	17346.415	19677.998	19672.627
13052.740	13049.171	14740.015	14735.988	15890.033	15885.693	17359.686	17354.946	19698.937	19693.561
13085.264	13081.686	14755.589	14751.557	15897.211	15892.869	17382.906	17378.160	19702.083	19696.706
13127.822	13124.233	14772.383	14768.347	15932.210	15927.858	17384.705	17379.958	19734.920	19729.534
13156.793	13153.196	14783.736	14779.697	15972.596	15968.233	17386.695	17381.948	19737.500	19732.113
13210.848	13207.236	14799.240	14795.196	16030.831	16026.453	17427.045	17422.287	19751.514	19746.123
13236.516	13232.897	14800.423	14796.379	16079.753	16075.361	17449.967	17445.203	19771.862	19766.466
13301.917	13298.280	14805.789	14801.744	16128.608	16124.203	17501.228	17496.450	19839.728	19834.313
13324.135	13320.492	14833.093	14829.040	16194.615	16190.192	17505.897	17501.117	19891.355	19885.926
13325.231	13321.588	14864.397	14860.336	16235.376	16230.942	17528.254	17523.468	19892.967	19887.538
13401.246	13397.582	14886.165	14882.098	16270.318	16265.874	17530.475	17525.689	19923.512	19918.075
13420.836	13417.167	14887.699	14883.631	16279.727	16275.281	17649.853	17645.034	19926.654	19921.216
13422.235	13418.566	14908.278	14904.205	16302.278	16297.826	17653.222	17648.402	20005.015	19999.555
13509.129	13505.436	14909.776	14905.702	16315.515	16311.059	17660.234	17655.412	20008.163	20002.703

Table 3. (continued)

λ_{vac}	λ_{air}	λ_{vac}	λ_{air}
20024.830	20019.365	21176.557	21170.779
20033.211	20027.744	21232.424	21226.630
20057.585	20052.111	21249.592	21243.794
20068.995	20063.518	21278.219	21272.413
20103.036	20097.550	21279.893	21274.086
20115.931	20110.441	21316.180	21310.364
20174.564	20169.058	21319.652	21313.835
20193.227	20187.716	21325.973	21320.154
20275.839	20270.306	21505.044	21499.176
20339.497	20333.946	21507.308	21501.440
20412.680	20407.110	21528.663	21522.789
20499.364	20493.770	21537.522	21531.645
20562.953	20557.342	21544.777	21538.898
20564.143	20558.531	21548.949	21543.069
20672.844	20667.203	21567.779	21561.894
20728.170	20722.514	21580.642	21574.754
20729.859	20724.202	21622.180	21616.280
20860.246	20854.554	21637.229	21631.325
20908.451	20902.746	21707.826	21701.903
20910.686	20904.980	21711.170	21705.246
21012.298	21006.564	21802.312	21796.363
21026.231	21020.494	21873.518	21867.550
21033.264	21027.525	21955.637	21949.647
21053.423	21047.678	22052.366	22046.349
21062.093	21056.346	22124.875	22118.838
21067.935	21062.186	22126.160	22120.123
21096.602	21090.845	22247.809	22241.739
21104.275	21098.516	22311.799	22305.712
21107.104	21101.345	22313.650	22307.562
21115.856	21110.094	22460.264	22454.136
21156.116	21150.343	22516.727	22510.584

Since it was necessary to extend slightly the data set published by these authors (for one ^{R}Q and one Q line and several $^{Q}P/^{Q}R$, P, ^{P}Q and ^{O}P lines) we used the wavenumbers given for the ^{S}R and R lines and the energy differences between the F_2 states and the F_1 and F_3 states (with respect to F_2 states). For the energy differences we used the results published by Babcock & Herzberg (1948). All the wavelengths published here can be considered secure to a few hundredths of Å.

Finally, we have computed the air wavelengths for all the OH lines identified in Figs. 3 to 23 (for the oxygen lines this conversion is already given in Table 2). This conversion is based on the formulae given in Allen (1973) and the results are reported Table 3.

5. Conclusion

In this paper we have extended the atlas of OH lines into the near-infrared domain, up to 2.25 μm. Since OH (and O_2 lines) are naturally imprinted on all near-infrared spectra obtained from the ground, this atlas represents a convenient tool for performing wavelength calibration without resorting to comparison arc spectra, and is routinely used for reducing ISAAC spectra.

The material used and presented in this paper is available for general use on the web at http://www.eso.org/instruments/isaac. Together with the Figs. 3 to 23 of this paper, the theoretical list of OH lines (including approximate relative intensities) used in this work is also available.

References

Abrams M.C., Davis S.P., Rao M.L.P., Engleman R. Jr., Braults J.W., 1994, ApJS 93, 351

Allen C.W., 1973, Astrophysical quantities. University of London, The Athlone Press

Anlauf K.G., MacDonald R.C., Polanyi J.C., 1968, Chem. Phys. Letters 1, 619

Babcock H.D., Herzberg L., 1948, ApJ 108, 167

Bunn F.E., Gush H.P., 1972, Can. J. Phys. 50(3), 213

Gush H.P., Buijs H.L., 1964, Can. J. Phys. 42, 1037

Herzberg L, Herzberg G., 1947, ApJ 105, 353

Maihara T., Iwamuro F., Yamashita T., et al., 1993, PASP 105, 940

Mies F.H., 1974, J. Mol. Spec. 53, 150

Moorwood A., Cuby J.-G., Ballester P., et al., 1999, Messenger, 95, 1.

Oliva E., Origlia L., 1992, A&A 254, 466

Osterbrock D.E., Fulbright J.P., Martel A.R., Keane M.J., Trager S.C., 1996, PASP 108, 277

Osterbrock D.E., Fulbright J.P., Bida T.A., 1997, PASP 109, 614

Osterbrock D.E., Donald E., Fulbright J.P., Cosby P.C., Barlow T.A., 1998, PASP 110, 1499

Wallace L., 1962, J. of the Atmos. Sciences 19 (1), 1

Wallace L., 1968, In: International Dictionary of Geophysics, pp. 1088-1094, Pergamon Press

Wyatt P.J., Stull V.R., Plass G.N., 1964, Applied Optics 3 (2), 229